PAPER

Untrasmall Bi$_2$S$_3$ nanodots for *in vivo* X-ray CT imaging-guided photothermal therapy of cancer†

Zelun Li,‡[a] Kelong Ai,‡[a] Zhe Yang,[b] Tianqi Zhang,[b] Jianhua Liu [ID] *[b] and Xiaoqiang Cui*[a]

Theranostic nanomedicine has shown tremendous promise for more effective and predictive cancer treatment by real-time mornitoring of the delivery of therapeutics to tumors and subsequent therapeutic response. However, the preparation of the theranostic nanoplatforms generally involves complicated procedures to encapsulate the therapeutic and imaging agents into a single nanoformulation. In this work, we develop an innovative nanotheranostic composed of ultrasmall PEG–Bi$_2$S$_3$ nanodots for simultaneous X-ray CT imaging and photothermal therapy. These nanodots possess several unique features: (i) efficient conversion of the NIR light into heat upon laser irradiation; (ii) long circulation time *in vivo* for effective tumor accumulation; (iii) 100% tumor elimination upon NIR laser irradiation in a tumor xenograft mouse model following systemic injection without obvious side effects; (iv) small size for efficient clearance from the body; and (v) high-performance CT imaging *in vivo* for potential imaging-guided therapy and the selection of cancer patients with high tumor accumulation. These results strongly suggest that this theranostic nanomedicine may become an effective tool for CT imaging-guided therapy for personalized cancer treatment.

1. Introduction

Nanotheranostics, which incorporates imaging and therapeutic agents into a single nanoformulation so that the therapy can be monitored noninvasively and in real time, has become a fast-growing and effective tool in the treatment of various diseases including cancers.[1] To date, enormous efforts have been made to fabricate nanotheranostics by the combination of varieties of imaging models and therapies.[2–6] Among them, the amalgamation of X-ray CT imaging with photothermal therapy has been considered to be one of most promising strategies for cancer treatment. Compared to other imaging tools, X-ray CT imaging is a widely used imaging tool in clinical diagnosis due to its deep tissue penetration and high resolution.[7,8] It is capable of providing the whole anatomic information of tumor tissues, including location, size, shape, and detecting if cancer spread has occured.[9,10] On the other hand, photothermal therapy (PTT) is known to specifically treat the tissue of interest in a spatial-, temporal-, and dosage-controlled fashion, with minimal invasiveness.[11–13] An ideal CT/PTT dual-functional nanomaterials should possess at least the following features: (i) high X-ray

attenuation ability; (ii) broad absorbance in the NIR region; (iii) long circulation time *in vivo* and effective accumulation in the tumor tissues; (iv) good biocompatibility; (v) the nanoparticles by themselves can serve as both imaging and PTT agents for simplifying the synthesis for reproducing; and (vi) robust fabrication processes that are amenable to scale-up for industry translation.

Bismuth sulfide (Bi$_2$S$_3$) nanostructures hold great promise for CT contrast agents, as Bi possesses larger X-ray attenuation coefficient than iodine,[14] the main CT contrast agent used in clinical imaging. More impressively, Bi$_2$S$_3$ has good biocompatibility and leaves no residue in the organism.[15] Additionally, it is more or less cost effective than currently studied heavy element-based nanoparticulate CT contrasts (*e.g.* Au, Pt, and Ta). It is also worth noting that Bi$_2$S$_3$ is a semiconductor with an energy gap of 1.33 eV. Such a low energy gap intrinsically enables Bi$_2$S$_3$ to exhibit strong absorbance in the NIR region.[16] Thus, Bi$_2$S$_3$ by itself can serve as a high-performance CT/PTT dual-functional agent without the need of additional combination of other functionalities. Few studies have thus far investigated the photothermal effect of Bi$_2$S$_3$ nanomaterials by themselves or through formation of nanocomposites with other nanomaterials (*e.g.* graphene and MoS$_2$),[17–20] and only two of them, to the best of our knowledge, reported the Bi$_2$S$_3$ nanomaterials as CT/PTT agents for cancer treatment.[19,20] However, Bi$_2$S$_3$ nanomaterials in these two studies have large particle sizes, which will have long retention time *in vivo* and may not penetrate into the deep tumor tissues, potentially leading to

[a]State Key Lab Automot Simulat & Control, Dept Mat Sci, Jilin Univ, Changchun 130012, P. R. China. E-mail: xqcui@jlu.edu.cn

[b]Department of Radiology, The Second Hospital of Jilin University, Changchun 130041, P R China. E-mail: drliujh@yahoo.com

† Electronic supplementary information (ESI) available. See DOI: 10.1039/c7ra04132b

‡ Kelong Ai and Zelun Li contributed equally to this work.

insufficient and heterogeneous hypothermia when the laser irradiation is taken.

Herein, we have developed ultrasmall PEG–Bi$_2$S$_3$ nanodots as a novel CT/PTT agent and systemically investigated their *in vivo* CT imaging and PTT therapeutic effect. Results demonstrated that PEG–Bi$_2$S$_3$ nanodots have small size, long circulation time *in vivo*, and high tumor accumulation. Following NIR laser irradiation, PEG–Bi$_2$S$_3$ nanodots efficiently converted the NIR light into heat, leading to hundred percent of tumor elimination and suppressing the tumor reoccurrence, with negligible side effects. In addition, PEG–Bi$_2$S$_3$ nanodots have demonstrated high-performance CT contrast efficacy *in vivo*, which can be potentially used for real-time and non-invasive tracking the behavior of PEG–Bi$_2$S$_3$ nanodots and identifying the patients who are most likely benefit the nanotherapeutics, given the tumor heterogeneity in different patients. We expected that PEG–Bi$_2$S$_3$ nanodots may be used as a simple but powerful theranostic nanoplatform for imaging-guided photothermal therapy for predictive and efficient cancer treatment.

2. Materials and method

2.1 Materials

Oleic acid, oleylamine, octadecance, thioacetamide, and bismuth neodecanoate were purchased from Sigma Aldrich. Poly(vinylpyrrolidone) 8000 was purchased from Alfa Aesar. Iobitridol was purchased from Guerbet (France). All the agents were used without additional purification.

2.2 Synthesis of oleic acid-stabilized Bi$_2$S$_3$ nanodots

Oleic acid-stabilized Bi$_2$S$_3$ nanodots were prepared according to previously reported method.[15] In brief, in a typical experiment, bismuth neodecanoate (7.2 g) was dissolved in the solution containing oleic acid (40 mL) and octadecene (80 mL) under vigorous stirring. The mixture was then slowly heated to 165 °C and then kept at this temperature for 20 min under Ar protection. After cooling down to 105 °C, 7 mL of oleyl amine solution containing thioacetamide (0.75 g) was rapidly injected into the mixture under vigorous stirring and Ar protection. The solution immediately turned dark brown upon injection of the thioacetamide. After reaction for 1 min, the mixture was allowed to cool down to the room temperature. Thereafter, ethanol was added, and oleic acid-stabilized Bi$_2$S$_3$ nanodots were obtained after centrifugation and washed twice with ethanol. The isolated oleic acid-stabilized Bi$_2$S$_3$ nanodots were redispersed in chloroform for further modification.

2.3 PEGylation of oleic acid-stabilized Bi$_2$S$_3$ nanodots

PEGylation was carried out according to a previously reported method with some modification.[8,21] In brief, 20 mL DSPE–PEG 2000 dissolved in chloroform (10 mg mL^{-1}) was mixed with 10 mL oleic acid-stabilized Bi$_2$S$_3$ nanodots dispersed in chloroform (2 mg mL^{-1}) for 10 min under general stirring. Thereafter, the chloroform was evaporated under vacuum at room temperature, followed by slowly heating to 60 °C to stabilize the interaction between DSPE–PEG and oleic acid. The resulting PEG-

coated Bi$_2$S$_3$ nanodots were then resuspended in 10 mL DI water, sonicated, and filtered using 0.2 μm filter. After centrifugation at 10 000 rpm for 20 min, the isolated PEG-coated Bi$_2$S$_3$ nanodots were redispersed in DI water for further characterization.

2.4 *In vitro* cytotoxicity of PEG-coated Bi$_2$S$_3$ nanodots

The cytotoxicity of PEG-coated Bi$_2$S$_3$ nanodots was examined by MTT assay. Briefly, 4T1 cells were cultured and seeded in the 96 well plates in RPMI-1640 supplemented with 10% FBS at 37 °C in an atmosphere of 5% CO$_2$ and 95% air. 24 hours later, the medium was replaced by fresh medium containing different concentrations of PEG-coated Bi$_2$S$_3$ nanodots for another 24 hours. The cell variability was then tested by MTT assay.

To further demonstrate the biocompatibility of PEG-coated Bi$_2$S$_3$ nanodots, cell viability of 4T1 cells treated with other PTT agents including CNT, GO, CuS, and CdSe nanoparticles at a concentration of 2 mg mL^{-1} were also examined using the MTT assay.

2.5 Blood biocompatibility of PEG-coated Bi$_2$S$_3$ nanodots

Human complete blood stabilized by EDTA was kindly provided by Second Hospital of Jilin University. 5 mL EDTA-stabilized human complete blood was added into 10 mL PBS, and centrifuged at 9000 rpm for 10 min. After washing with PBS five times, red blood red cells were diluted by 50 mL PBS. Thereafter, 0.4 mL of red blood cell solution was mixed with 1.6 mL of PBS containing different concentrations of PEG-coated Bi$_2$S$_3$ nanodots, PBS alone (negative control), and deionized water (positive control), respectively. After incubation at room temperature for 3 hours, the samples were centrifuged at 12 000 rpm for 20 min. The absorbance of the supernatants at the wavelength of 541 nm was examined using a UV-vis spectroscopy. The hemolysis of PEG-coated Bi$_2$S$_3$ nanodots was calculated according to the following equation: hemolysis% = $(A_{sample} - A_{(-)control})/(A_{(+)control} - A_{(-)control})$

2.6 *In vitro* photothermal conversion performance

To evaluate the photothermal conversion effect of the PEG-coated Bi$_2$S$_3$ nanodots, 1 mL aqueous dispersion of PEG-coated Bi$_2$S$_3$ nanodots at different concentrations (75, 148, 276, and 387 μg mL^{-1}) was respectively added in a quartz cuvette and irradiated with an 808 nm NIR laser at a power density of 3 W cm^{-2} for 500 s. A thermocouple probe with an accuracy of 0.1 °C was inserted into the PEG-coated Bi$_2$S$_3$ nanodots aqueous solution perpendicular to the path of the laser. The temperature was recorded every 10 s by a digital thermometer with a thermocouple probe.

2.7 Photothermal cytotoxicity

In vitro photothermal cytotoxicity of PEG-coated Bi$_2$S$_3$ nanodots was assessed using 4T1 murine breast cancer cells. Briefly, 4T1 cells were cultured in 6-well plates at 37 °C for 24 h, and then incubated with PEG-coated Bi$_2$S$_3$ nanodots at a concentration of 75, 150, or 300 μg mL^{-1} for 30 min. After irradiation with an

808 nm laser at a power density of 3 W cm^{-2} for 5 min, the cells were stained with both calcein AM (calcein acetoxymethyl ester) and PI (propidium iodide), and the cell death was observed using a confocal fluorescence microscope.

2.8 Tumor xenograft model

Animals were maintained in accordance with the guidelines of the Standardization Administration of the People's Republic of China, and approved by the institutional ethical committee (IEC) of the Second Hospital of Jilin University. For the xenograft tumor models, 4T1 cells were cultured in RPMI-1640 supplemented with 10% FBS at 37 °C in an atmosphere of 5% CO$_2$ and 95% air. 2×10^6 4T1 cells were suspended in 100 μL serum-free culture medium and then inoculated subcutaneously into the bilateral flanks of female Balb/C mice. The mice were used for further experiments when the tumor size has achieved to 5 mm in diameter.

2.9 *In vivo* photothermal therapy

For observation of *in vivo* photothermal therapy effect of PEG-coated Bi$_2$S$_3$ nanodots, 4T1 tumor bearing mice were first anesthetized by intraperitoneal injection of chloral hydrate solution (10 wt%) and intratumorally injected with 50 μL PEG-coated Bi$_2$S$_3$ nanodots aqueous dispersion (200 μg mL^{-1}). Subsequently, the tumors were irradiated with an 808 nm laser at 3 W cm^{-2} for 5 min.

For intravenous injection of PEG-coated Bi$_2$S$_3$ nanodots, tumor-bearing mice were injected with PEG-coated Bi$_2$S$_3$ nanodots through the tail vein, and exposed to laser irradiation at 24 h postinjection of PEG-coated Bi$_2$S$_3$ nanodots.

The tumor sizes were measured by a caliper every other day and calculated as the volume according to the following equation:

$$\text{Tumor volume} = (\text{tumor length}) \times (\text{tumor width})^2/2.$$

Relative tumor volumes were calculated as V/V_0 (V_0 was the tumor volume when the treatment was initiated).

2.10 Blood analysis

Healthy mice were intravenously administered with a single dose of PEG-coated Bi$_2$S$_3$ nanodots. Several healthy mice were also used as the control group. The mice were anesthetized and the blood was collected by a cardiac puncture method for blood biochemistry assay.

2.11 *In vivo* CT imaging

Tumor-bearing mice were first anesthetized by intraperitoneal injection of chloral hydrate solution (10 wt%), and then intravenously injected with PEG-coated Bi$_2$S$_3$ nanodots dispersion in PBS (200 μL, 20 mg Bi per mL) through the tail vein. The whole body CT imaging was performed using clinical CT scanner with the parameters: thickness, 0.9 mm; pitch, 0.99; 120 kVp, 300 mA; field of view, 350 mm; gantry rotation time, 0.5 s; table speed, 158.9 mm s^{-1}.

Animal care and handing procedures were in agreement with the guidelines of the Regional Ethics Committee for Animal Experiments.

2.12 Characterization

The morphology of PEG-coated Bi$_2$S$_3$ nanodots was characterized by using a TECNAI G2 high-resolution transmission electron microscope and a FEI/Philips XL30 ESEM FEG field-emission scanning electron microscope. XRD patterns were collected on a D8 ADVANCE (Germany) using Cu Kα (0.15406 nm) radiation.

3. Results and discussion

3.1 Synthesis and characterization of PEG-coated Bi$_2$S$_3$ nanodots

The ultrasmall oleic acid-stabilized Bi$_2$S$_3$ nanodots were synthesized through a "hot injection" method. Briefly, the oleylamine solution containing thioacetamide was rapidly injected into the hot octadecane solution containing bismuth neodecanoate and oleic acid at 105 °C under vigorous stirring, followed by heating to 165 °C and keeping at this temperature for 20 min under Ar protection. Thioacetamide can desulfurize at this temperature and react with bismuth neodecanoate to form Bi$_2$S$_3$ nanodots. The resulting Bi$_2$S$_3$ nanodots can be well dispersed in different organic solvents such as cyclohexane, chloroform, and dichloromethane, and remained stable even after repeated washing, without any detectable aggregation. In our previous study, we used polyvinylpyrrolidone (PVP) as the exchanging ligand to make the Bi$_2$S$_3$ nanodots water soluble,[15] whereas the PVP-modified Bi$_2$S$_3$ nanodots exhibited high viscosity at high concentrations. To address this issue, here we used amphiphilic 1,2-distearoyl-*sn-glycero*-3-phosphoethanolamine-*N*-[amino(polyethylene glycol)] (DSPE–PEG) for modification of Bi$_2$S$_3$ nanodots through the hydrophobic interaction between DSPE–PEG and oleic acid to reduce the non-specific absorption and thus improve their physiological stability. As shown in Fig. 1a, PEG-coated Bi$_2$S$_3$ nanodots were 3–4 nm in size and well dispersed in water without obvious aggregation. The Bi$_2$S$_3$ crystal structure was confirmed by X-ray powder diffraction (XRD) analysis (Fig. 1b). In addition, PEG-coated Bi$_2$S$_3$ nanodots showed a linear concentration-dependent increase in the absorbance in the NIR region (Fig. 1c and d), suggesting the great potential of PEG-modified Bi$_2$S$_3$ nanodots for NIR-mediated photothermal therapy.

3.2 Cytotoxicity of PEG-coated Bi$_2$S$_3$ nanodots

To assess the cytotoxicity of PEG-coated Bi$_2$S$_3$ nanodots, 4T1 cancer cells were incubated with different concentrations of PEG-coated Bi$_2$S$_3$ nanodots for 24 h, and the cell viability was compared to the control cells using MTT assay. As illustrated in Fig. 2a, treatment of PEG-coated Bi$_2$S$_3$ nanodots did not induce obvious toxicity in 4T1 cells at a concentration up to 2 mg mL^{-1}. To better demonstrate the potential of PEG-coated Bi$_2$S$_3$ nanodots as a biocompatible PTT agent, we compared the cytotoxicity of PEG-coated Bi$_2$S$_3$ nanodots with several other PTT
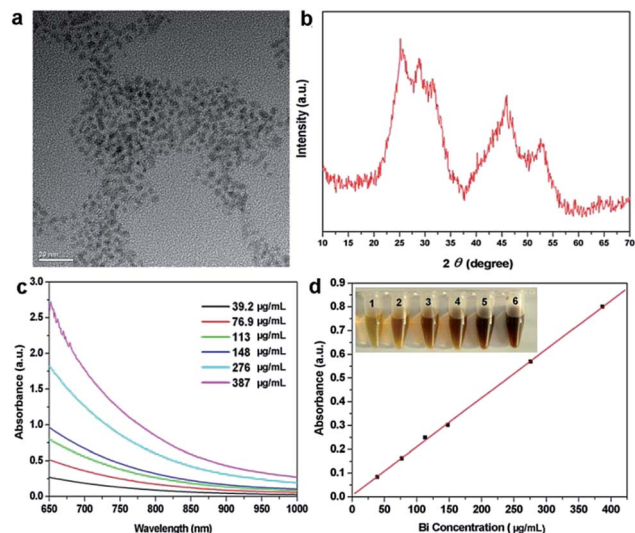
Fig. 1 (a) TEM image of PEG-coated Bi_2S_3 nanodot aqueous solution and (b) XRD spectrum of PEG-coated Bi_2S_3 nanodots. (c) UV-vis-NIR spectra of PEG-coated Bi_2S_3 nanodot aqueous solutions at different concentrations. (d) The absorbance at 808 nm of PEG-coated Bi_2S_3 nanodot aqueous solutions at different concentrations. The insert is the corresponding picture. From 1 to 6: PEG-coated Bi_2S_3 nanodot aqueous solutions at increasing concentrations shown in (d).
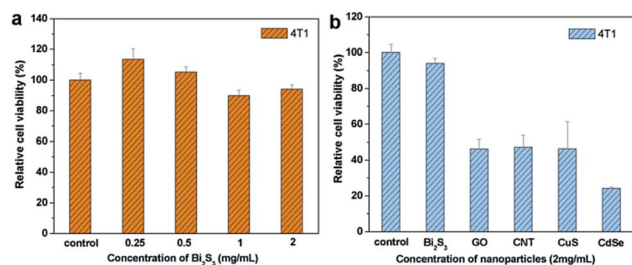

Fig. 2 (a) Cell viability of 4T1 cells after incubation of different concentrations of PEG-coated Bi_2S_3 nanodots for 24 h. (b) Cell viability of 4T1 cells treated with PEG-coated Bi_2S_3 nanodots, CNT, GO, CuS, and CdSe nanomaterials at the same concentration (2 mg mL^{-1}).

agents including graphene oxide (GO), carbon nanotube (CNT), CuS, and CdSe nanomaterials. Only half of cells treated with GO, CNT, or CuS remained alive at a concentration of 2 mg mL^{-1}, and almost 80% cells died after treatment with CdSe nanomaterials at the same concentration, which is largely due to the released Cd^{2+} and Se^{2+} ions from CdSe nanomaterials.[22,23] These results clearly suggested the low cytotoxicity of PEG-coated Bi_2S_3 nanodots.

To further evaluate the biocompatibility of PEG-coated Bi_2S_3 nanodots, we examined the blood compatibility of PEG-coated Bi_2S_3 nanodots, which is an important evaluation index to see if the newly developed nanomaterials are applicable for *in vivo* applications. Similar to the PBS negative control group, no hemolysis was noticed after incubation of blood with PEG-coated Bi_2S_3 nanodots, even at a concentration of 2 mg mL^{-1}, in sharp contrast to the water positive control group, suggesting the good blood compatibility of PEG-coated Bi_2S_3 nanodots

(Fig. S1†). All these results strongly suggested that PEG-coated Bi_2S_3 nanodots can be used as a safe PTT agent for *in vivo* applications.

3.3 Photothermal conversion and photostability

To evaluate the potential of PEG-coated Bi_2S_3 nanodots in PTT therapy, we first tested their photothermal conversion capability. PEG-coated Bi_2S_3 nanodots were dispersed in water at different concentrations, and exposed to an 808 nm laser for 500 seconds at a power density of 3 W cm^{-2}. The temperature was then monitored. For comparison, the temperature change of pure water was also monitored at the same condition (Fig. 3). Clearly, the temperature of pure water was increased by less than 3 °C after 500 s of laser irradiation. In contrast, the temperature of PEG-coated Bi_2S_3 nanodot aqueous solutions showed a dose-dependent increase upon laser irradiation. At a concentration of 276 μg mL^{-1}, the temperature of PEG-coated Bi_2S_3 nanodot aqueous solution increased to 34.3 °C. Further increase in the concentration of PEG-coated Bi_2S_3 nanodots did not lead to more enhanced temperature increase, which was presumably due to the saturated nanodots compared to the laser irradiation. More impressively, PEG-coated Bi_2S_3 nanodots demonstrated excellent photostability: no change in size, morphology, or absorbance in the NIR region was visualized during 1 h continuous laser irradiation (Fig. S2 and S3†). The photothermal conversion efficiency was calculated to be ~21% according to previous work (Fig. S3†).[24]

3.4 *In vitro* photothermal therapy

The high photothermal conversion of PEG-coated Bi_2S_3 nanodots makes them feasible to be a PTT agent for cancer therapy. To further demonstrate the photothermal effect of PEG-coated Bi_2S_3 nanodots, 4T1 cells were incubated with PEG-coated Bi_2S_3 nanodots and then exposed to laser irradiation with an 808 nm laser at a power density of 3 W cm^{-2} for 5 min, followed by staining with calcein AM and PI. Cells without treatment or with treatment of lase alone were also stained with calcein AM and PI as the control groups. Fig. 4 demonstrated that nearly no cells died when laser was taken alone, whereas a dose-dependent cell death was observed for cells treated with PEG-coated Bi_2S_3 nanodots, coupled with laser irradiation. Almost
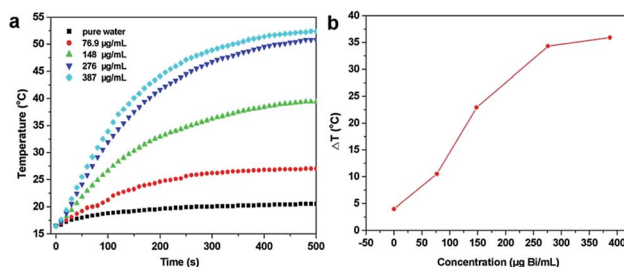

Fig. 3 (a) Temperature increase of PEG-coated Bi_2S_3 nanodot aqueous solutions at different concentrations upon laser irradiation with an 808 nm laser at a power density of 3 W cm^{-2}. (b) The corresponding maximum temperature change.
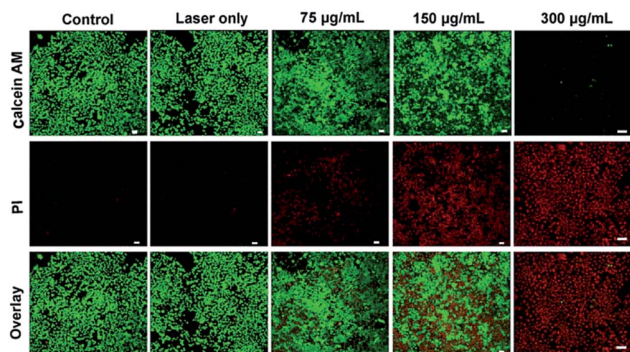
Fig. 4 Confocal fluorescence images of calcein AM (green, live cells) and propidium iodide (red, dead cells) co-stained 4T1 cells treated with different concentrations of PEG-coated Bi_2S_3 nanodots, followed by laser irradiation for 5 min. The power density is 3 W cm^{-2}. The scale bar is 50 μm.

all the cells died at a concentration of 300 μg mL^{-1} after laser irradiation, which was consistent with the quantitative cell viability analysis (Fig. S4†). These results clearly indicated the potential of PEG-coated Bi_2S_3 nanodots for cancer PTT therapy.

3.5 *In vivo* CT imaging of tumor

Imaging function in theranostics can be used for real-time tracking *in vivo* pharmacokinetics and biodistribution of therapeutics. One of the advantages of PEG-coated Bi_2S_3 nanodots compared to currently studied CT/PTT is that PEG-coated Bi_2S_3 nanodots by themselves can be used as both imaging and therapy, thus simplifying the synthesis. Moreover, superior to Au nanostructures, which also have both imaging and therapeutic functions, Bi is much less expensive than Au, revealing that this strategy had great potential for industrial production.

To examine the *in vivo* CT imaging performance, PEG-coated Bi_2S_3 nanodots were then intravenously injected in the mouse and the whole body CT imaging was carried out. Differing from the commercial iodine-based small molecule CT contrast agents, which will be cleared from the blood within seconds to minutes due to their low molecular weights, PEG-coated Bi_2S_3 nanodots showed prolonged circulation time in the blood. Enhanced CT signals were observed for different organs. There is an increased CT contrast in the heart upon injection, even after 1 h postinjection (Fig. 5). The prolonged circulation time will enable PEG-coated Bi_2S_3 nanodots to accumulate in the tumor through enhanced permeability and retention effect (EPR) effect. It is worth nothing that high CT signal was observed in the bladder, clearly suggesting that Bi_2S_3 nanodots can be efficiently eliminated from the body through the kidney, due to the small size. The CT value of each organ has been summarized in Table S1,† which provided further evidence for the CT contrast compared to pre-injection.

4T1 xenograft tumor model was then set up by subcutaneously injection of 4T1 cells suspended in serum-free culture medium into the bilateral flanks of healthy Balb/C mice to evaluate if the nanodots are able to accumulate in tumor through the EPR effect. We also quantified the CT values of tumor before *vs.* after injection of PEG-coated Bi_2S_3 nanodots.
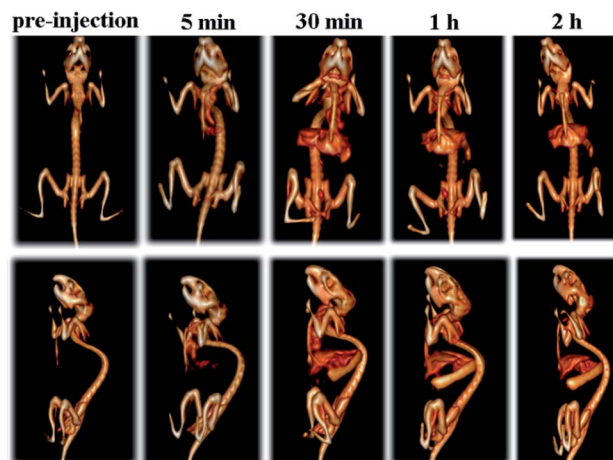

Fig. 5 Time-dependent whole body CT imaging of the mouse after intravenous injection of PEG-coated Bi_2S_3 nanodots.
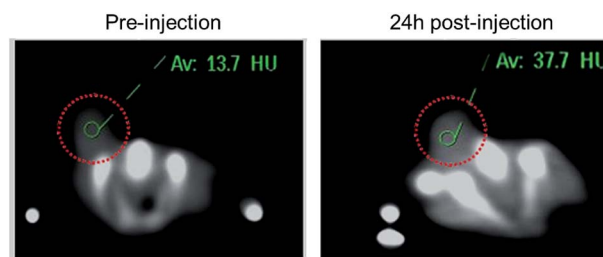

Fig. 6 CT images of 4T1 tumor-bearing mouse before and at 24 h postinjection of PEG-coated Bi_2S_3 nanodots through the tail vein.

At 24 hours postinjection, the CT value of the tumor increased by approximately 3 times, as compared to the CT value of tumor before injection (Fig. 6). All these results clearly suggested that PEG-coated Bi_2S_3 nanodots can be used for imaging-guided therapy and potentially determination of the tumor EPR effect to identify those patients most likely to benefit the nanotherapeutics. We also noted that the tumor site become dark after injection of PEG-coated Bi_2S_3 nanodots compared to pre-injection (Fig. S5†), providing further evidence for the accumulation of PEG-coated Bi_2S_3 nanodots. ICP analysis further confirmed the high accumulation of PEG-coated Bi_2S_3 nanodots in the tumor site (Fig. S6†). Small molecule-based CT contrast agents are known to passage out of tumor due to the small molecule weight. The short retention makes it hard for long-term monitoring the histological analysis of tumor. To better examine the retention effect of our PEG-coated Bi_2S_3 nanodots, PEG-coated Bi_2S_3 nanodots were directly injected in the tumor, and the time-dependent CT imaging of tumor was performed. As shown in Fig. 7, bright CT signal remained even at 30 min postinjection.

3.6 *In vivo* photothermal therapy

Given the excellent photothermal efficiency and effective tumor accumulation and retention, we proceeded to assess the *in vivo*
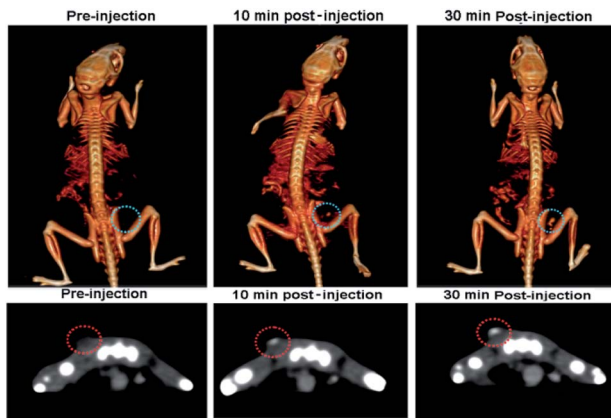
Fig. 7 Time-dependent CT images of the tumour after intratumoral injection of PEG-coated Bi_2S_3 nanodots.

photothermal therapy effect of PEG-coated Bi_2S_3 nanodots. PEG-coated Bi_2S_3 nanodots were injected into 4T1 tumor-bearing mice intravenously or intratumorally, and the tumors were irradiated with a 808 nm laser for 5 min at a power density of 3 W cm^{-2}. As illustrated in Fig. 8a, the tumors were eliminated for mice treated with PEG-coated Bi_2S_3 nanodots upon laser irradiation, regardless of the injection route. No tumor recurrence was observed (Fig. 8b). In contrast, the control mice showed fast tumor growth. During one-month period of observation, mice remained healthy, and no abnormalities in eating, drinking, grooming, activity, exploratory behavior, urination, or neurological status were noticed. The body weight

Fig. 8 (a) Digital pictures of the control 4T1 tumor-bearing mouse and 4T1 tumor-bearing mice after injection of PEG-coated Bi_2S_3 nanodots. (b) Tumor growth curve of 4T1 tumor-bearing mice received different treatments. (c) Body weight changes of control mice and mice treated with PEG-coated Bi_2S_3 nanodots.

of the treated group gradually increased in a manner similar to that of the control groups (Fig. 8c).

3.7 *In vivo* toxicity studies of PEG-coated Bi_2S_3 nanodots

Finally, the potential *in vivo* side effects of PEG-coated Bi_2S_3 nanodots were also examined. PEG-coated Bi_2S_3 nanodots were injected into healthy mice at a single dose injection, and the blood was withdrawn for blood analysis. Results showed that the five important hepatic indicators including aspartate transaminase (AST), alanine transaminase (ALT), alkaline phosphatase (ALP), total protein (TP) and albumin/globin ratio (A/G) fell within normal ranges and thus revealed no sign of liver injury. Complete blood tests demonstrated no obvious interference with the physiological regulation of haem or triggering the immune responses (Fig. S7†).

4. Conclusions

In this work, we have described an innovative nanotheranostic based on PEG-coated Bi_2S_3 nanodots with uniform size, good dispersibility in water, and strong NIR absorbance. They have shown long circulation time *in vivo* and can effectively accumulate in tumor through the EPR effect with long retention time. Upon laser irradiation with an 808 nm laser, PEG-coated Bi_2S_3 nanodots can efficiently convert the NIR light into heat to generate hyperthermia and thus suppress the tumor growth. In addition, the high X-ray attenuation of Bi enables PEG-coated Bi_2S_3 nanodots to be a CT contrast agent for potential and real-time tracking the *in vivo* behavior of PEG-coated Bi_2S_3 nanodots for theranostic treatment of cancer. We expect PEG-coated Bi_2S_3 nanodots to provide a new tool for imaging-guided photothermal therapy of various diseases including cancers.

Acknowledgements

Notes and references

1 K. Y. Choi, G. Liu, S. Lee and X. Chen, *Nanoscale*, 2012, **4**, 330–342.

2 F. M. Kievit and M. Zhang, *Adv. Mater.*, 2011, **23**, H217–H247.

3 X. Ma, Y. Zhao and X. J. Liang, *Acc. Chem. Res.*, 2011, **44**, 1114–1122.

4 P. Huang, J. Lin, W. Li, P. Rong, Z. Wang, S. Wang, X. Wang, X. Sun, M. Aronova, G. Niu, R. D. Leapman, Z. Nie and X. Chen, *Angew. Chem., Int. Ed.*, 2013, **52**, 13958–13964.

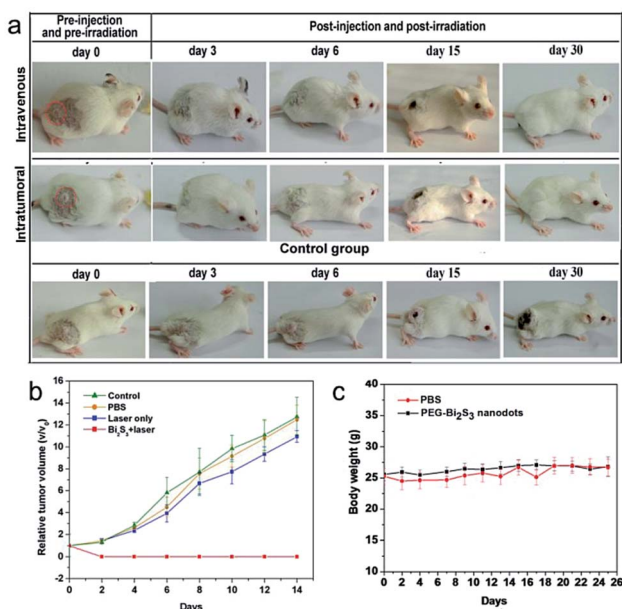5 K. Dong, Z. Liu, Z. Li, J. Ren and X. Qu, *Adv. Mater.*, 2013, **25**, 4452–4458.

6 Y. Liu, K. Ai, J. Liu, M. Deng, Y. He and L. Lu, *Adv. Mater.*, 2013, **25**, 1353–1359.

7 F. Hyafil, J. C. Cornily, J. E. Feig, R. Gordon, E. Vucic, V. Amirbekian, E. A. Fisher, V. Fuster, L. J. Feldman and Z. A. Fayad, *Nat. Med.*, 2007, **13**, 636–641.

8 Y. Liu, K. Ai, J. Liu, Q. Yuan, Y. He and L. Lu, *Angew. Chem., Int. Ed.*, 2012, **51**, 1437–1442.

9 H. Lusic and M. W. Grinstaff, *Chem. Rev.*, 2013, **113**, 1641–1666.

10 Y. Liu, K. Ai and L. Lu, *Acc. Chem. Res.*, 2012, **45**, 1817–1827.

11 L. Cheng, J. Liu, X. Gu, H. Gong, X. Shi, T. Liu, C. Wang, X. Wang, G. Liu, H. Xing, W. Bu, B. Sun and Z. Liu, *Adv. Mater.*, 2014, **26**, 1886–1893.

12 L. Zou, H. Wang, B. He, L. Zeng, T. Tan, H. Cao, X. He, Z. Zhang, S. Guo and Y. Li, *Theranostics*, 2016, **6**, 762–772.

13 D. Jaque, L. Martinez Maestro, B. del Rosal, P. Haro-Gonzalez, A. Benayas, J. L. Plaza, E. Martin Rodriguez and J. Garcia Sole, *Nanoscale*, 2014, **6**, 9494–9530.

14 O. Rabin, J. Manuel Perez, J. Grimm, G. Wojtkiewicz and R. Weissleder, *Nat. Mater.*, 2006, **5**, 118–122.

15 K. Ai, Y. Liu, J. Liu, Q. Yuan, Y. He and L. Lu, *Adv. Mater.*, 2011, **23**, 4886–4891.

16 L. Martinez, M. Bernechea, F. P. G. de Arquer and G. Konstantatos, *Adv. Energy Mater.*, 2011, **1**, 1029–1035.

17 R. Dou, Z. Du, T. Bao, X. Dong, X. Zheng, M. Yu, W. Yin, B. Dong, L. Yan and Z. Gu, *Nanoscale*, 2016, **8**, 11531–11542.

18 S. Wang, X. Li, Y. Chen, X. Cai, H. Yao, W. Gao, Y. Zheng, X. An, J. Shi and H. Chen, *Adv. Mater.*, 2015, **27**, 2775–2782.

19 J. Liu, X. Zheng, L. Yan, L. Zhou, G. Tian, W. Yin, L. Wang, Y. Liu, Z. Hu, Z. Gu, C. Chen and Y. Zhao, *ACS Nano*, 2015, **9**, 696–707.

20 Z. Li, Y. Hu, M. Chang, K. A. Howard, X. Fan, Y. Sun, F. Besenbacher and M. Yu, *Nanoscale*, 2016, **8**, 16005–16016.

21 B. Dubertret, P. Skourides, D. J. Norris, V. Noireaux, A. H. Brivanlou and A. Libchaber, *Science*, 2002, **298**, 1759–1762.

22 C. Kirchner, T. Liedl, S. Kudera, T. Pellegrino, A. Munoz Javier, H. E. Gaub, S. Stolzle, N. Fertig and W. J. Parak, *Nano Lett.*, 2005, **5**, 331–338.

23 R. Hardman, *Environ. Health Perspect.*, 2006, **114**, 165–172.

24 Y. Liu, K. Ai, J. Liu, M. Deng, Y. He and L. Lu, *Adv. Mater.*, 2013, **25**, 1353–1359.